Journal of Nanobiotechnology

RESEARCH

Open Access

Macrophage-derived extracellular vesicles represent a promising endogenous iron-chelating therapy for iron overload and cardiac injury in myocardial infarction

Dong Guo[1†], Xue Yang[1†], Rui Yu[1†], Jing Geng[1], Xiaoliang Zhang[1], Ying Wang[1], Qi Liang[1], Siying Pu[1], Tingwei Peng[1], Mingchuan Liu[1], Feng Fu[2], Zhelong Li[3], Lang Hu[1*] and Yan Li[1*]

Abstract

Background Cardiac iron overload and ferroptosis greatly contribute to the poor prognosis of myocardial infarction (MI). Iron chelator is one of the most promising strategies for scavenging excessive iron and alleviating cardiac dysfunction post MI. However, various side effects of existing chemical iron chelators restrict their clinical application, which calls for a more viable and safer approach to protect against iron injury in ischemic hearts.

Results In this study, we isolated macrophage-derived extracellular vesicles (EVs) and identified macrophage-derived EVs as a novel endogenous biological chelator for iron. The administration of macrophage-derived EVs effectively reduced iron overload in hypoxia-treated cardiomyocytes and hearts post MI. Moreover, the oxidative stress and ferroptosis induced by excessive iron were considerably suppressed by application of macrophage-derived EVs. Mechanistically, transferrin receptor (TfR), which was inherited from macrophage to the surface of EVs, endowed EVs with the ability to bind to transferrin and remove excess protein-bound iron. EVs with TfR deficiency exhibited a loss of function in preventing MI-induced iron overload and protecting the heart from MI injury. Furthermore, the iron-chelating EVs were ultimately captured and processed by macrophages in the liver.

Conclusions These results highlight the potential of macrophage-derived EVs as a powerful endogenous candidate for iron chelation therapy, offering a novel and promising therapeutic approach to protect against iron overload-induced injury in MI and other cardiovascular diseases.

Keywords Myocardial infarction, Iron overload, Macrophages, Extracellular vesicles, Iron chelating therapy, Transferrin receptor

[†]Dong Guo, Xue Yang, and Rui Yu contributed equally to this work.

*Correspondence:
Lang Hu
medhulang@163.com
Yan Li
profleeyan@163.com

[1]Department of Cardiology, Tangdu Hospital, Airforce Medical University, Xi'an 710032, China
[2]Department of Physiology and Pathophysiology, Airforce Medical University, Xi'an 710032, China
[3]Department of Ultrasound Diagnostics, Tangdu Hospital, Airforce Medical University, Xi'an 710032, China

Background

Myocardial infarction (MI) poses a substantial threat to public health worldwide [1]. Various pathological mechanisms contribute to cardiac ischemic injury, including inflammation, burst reactive oxygen species (ROS) production, cell apoptosis and iron overload. Among them, iron overload has been identified as a major detrimental factor that contributes to the poor prognosis of MI. During cardiac ischemic injury, iron derived from damaged cardiomyocytes, red blood cells and circulating transferrin-bound iron are deposited either in the extracellular matrix or within cardiomyocytes. Clinical studies have demonstrated that patients with ST-segment-elevation MI exhibit cardiac iron overload during follow-up [2], and animal models have confirmed the presence of excess iron in hypoxic cardiomyocytes and infarcted hearts [3]. Cellular iron overload can generate ROS such as hydroxyl radicals by reacting with hydrogen peroxide via the Fenton reaction. This process leads to ferroptosis and acute cardiomyocyte death [4, 5]. Moreover, chronic cardiac iron accumulation during the remodelling process has been associated with prolonged inflammation and pathological ventricular remodelling [2, 6]. These findings highlight the importance of promptly and effectively removing excess iron to limit myocardial injury and improve long-term prognosis in patients with MI.

To date, iron chelator is one of the most promising strategies for scavenging excessive iron and preventing the Fenton reaction. The iron chelators, such as deferoxamine (DFO), deferiprone (DFP) and deferasirox (DFX), can enter cells and bind intracellular labile iron to eliminate the excess iron. While the effectiveness of these chemical iron chelators has been widely established, their clinical application is limited by several drawbacks. For example, DFO's highly hydrophilic structure results in inadequate absorption bioavailability and rapid metabolic rate, necessitating prolonged infusion periods and negatively impacting patient compliance [7]. To address this issue, oral iron chelators, such as DFP and DFX, were developed. However, both DFP and DFX were associated with significant side effects, including gastrointestinal toxicities, renal dysfunction, liver damage, hypersensitivity reactions and neuronal hearing loss [8]. Thus, these limitations of chemical iron chelators call for further advancements in iron scavenging strategies. Moreover, instead of relying on exogenous chemical compounds, exploring and utilising endogenous biological iron chelation mechanisms could offer a viable approach to protect against iron injury in ischemic hearts while limiting side effects.

Macrophages, the primary regulators of iron metabolism, play a crucial role in systemic and organ-specific iron homeostasis. Macrophages have the ability to acquire iron from the extracellular environment through iron-binding protein receptors on their cell surface. Studies have reported that muscle-resident macrophages exhibited increased iron uptake and storage capacity during injury, thereby alleviating iron overload and promoting tissue repair [9]. These findings underscore the potential therapeutic value of macrophage activation in managing iron overload during acute injury. However, the overactivation and aggregation of macrophages at the injury site led to its participation in immune reactions and the aggravation of tissue damage after acute ischemia. Therefore, a key question arises regarding how to harness the iron-sequestering capacity of macrophages while simultaneously preventing macrophage-induced inflammation. A recent study reported that macrophage-derived extracellular vesicles (EVs) inherited membrane receptors from their parent cells [10], endowing EVs with the potential to retain macrophages' ability to handle iron. Compared to their parent cells, the higher surface-to-volume ratio of EVs enhances their ability to capture target substances. Thus, we hypothesise that macrophage-derived EVs could serve as endogenous iron chelators to alleviate myocardial iron overload and related injury in ischemic hearts.

In this study, we investigated the efficacy of EVs released by macrophages as an effective iron-sequestering agent. The administration of macrophage-derived EVs demonstrated a significant cardioprotective effect against MI and hypoxia treatment by reducing myocardial iron overload and ferroptosis. Mechanistically, we identified the transferrin receptor (TfR), inherited from macrophages to the surface of EVs, as a key contributor to the iron chelation capacity of EVs. EVs lacking TfR lost their ability to eliminate excess iron and protect the heart from MI injury. Additionally, we observed that iron-binding EVs were ultimately recycled by macrophages in the liver. Collectively, our work unveils a novel mechanism by which macrophages handle iron overload in MI hearts and identifies macrophage-derived EVs as a promising iron chelation therapy for the treatment of MI-induced iron overload and cardiac injury.

Methods

Animals

All animal experiments were approved by Animal Use and Care Committee of Air Force Medical University, and were conducted in compliance with ethical regulations of animal research. All mice used were provided by the animal center of Air Force Medical University, which were males in C57BL/6J background and were 6–8 weeks old at the onset of experiments. Mice were housed under controlled conditions of lighting (12 h light/12 h dark cycle), temperature (22±1℃), and humidity (60±5%) with free access to food and water.

Construction of MI model

MI was induced as previously described [11]. Briefly, mice were anesthetized with 2–3% isoflurane and hearts were exposed through the incision in the chest. Then, left anterior descending (LAD) coronary artery was ligated with 6−0 silk approximately 2–3 mm below the origin. After ligation, the heart was returned and the chest was closed. Mice in the sham group received same operation except LAD ligation. All mice were monitored for 3–6 h before returning to their normal animal room. The success of MI model construction was determined by histological staining and echocardiography.

Triphenyl tetrazolium chloride (TTC) staining

After anesthetization, the chest of mice was cut open to expose the heart. Then the heart was harvested, washed, and sectioned into approximately 1–2 mm thick sections. All sections were incubated with 1% TTC (A610558, Sangon Biotech) for 15 min at room temperature and then fixed in paraformaldehyde (A500684, Sangon Biotech). Image J was used to calculate the percentage of infarcted myocardium.

Echocardiography

Echocardiography was performed with VEVO 3100 echocardiography system (VisualSonics Inc., Toronto, Canada). Mice were anesthetized with pentobarbital sodium (intraperitoneal injection, 60 mg/kg body weight) or isoflurane (inhalation anesthesia, 2–3%). Anesthetization was adjusted to maintain the heart rate within 400–450 bpm. M-mode echocardiography was performed as previously described [12]. Left ventricular ejection fraction (LVEF), left ventricular fractional shortening (LVFS), left ventricular end-systolic volume (LVESV), and left ventricular end-diastolic volume (LVEDV) were calculated.

Measurement of creatine kinase (CK), creatine kinase MB (CKMB), lactate dehydrogenases (LDH), and LDH1

Mice were anesthetized with 2–3% isoflurane and the neck skin were cut open to expose carotid artery. Blood sample were immediately collected after carotid artery was cut. The collected blood sample were stored overnight at 4℃ and then centrifuged at 3000 rpm for 15 min at 4 °C. The supernatant was collected as serum. The amount of CK, CKMB, LDH, and LDH1 were determined using automatic biochemical analyzer (Chemray 240).

Measurement of iron level

The measurement of iron level in serum, myocardium lysate, cardiomyocyte culture medium, cardiomyocyte lysate, and solution of iron ion, was performed using Total Iron Colorimetric Assay Kit (Elabscience, E-BC-K772-M) following manufacturer's instructions. Briefly, the serum and cell culture medium sample were diluted and then tested. The heart and cardiomyocyte sample were homogenized, centrifuged, and then tested. The iron level was calculated based on the standard curve. To detect the iron level inside live cardiomyocytes, fluorescent iron probe FerroOrange (MaokangBio) was also used following manufacturer's instructions (data shown in Fig. 3a and b).

Western blotting

Ventricular tissue, cells or EVs were lysed with ice-cold RIPA buffer (Beyotime, P0013B). The protein concentration was then determined with Pierce BCA Protein Assay Kit (Thermo Scientific, 23225). Protein sample were separated by SDS-PAGE and transferred to nitrocellulose membrane. Membranes were blocked with skim milk, incubated with primary and secondary antibodies, and detected by chemiluminescent detection system (Image Lab, Bio-Rad, US). Equal protein loading would be confirmed with antibodies against β-Actin. Antibodies used in this study were listed below: anti- ferritin heavy chain 1 (FTH1) (Santa Cruz, sc-376594), anti-transferrin (Proteintech, 17435-1-AP), anti- glutathione peroxidase 4 (GPX4) (Santa Cruz, sc-166437), anti-β-Actin (Proteintech, 66009-1), HRP-conjugated Affinipure Goat Anti-Rabbit IgG(H+L) (Proteintech, SA00001-2), and HRP-conjugated Affinipure Goat Anti-Mouse IgG(H+L) (Proteintech, SA00001-1).

Immunohistochemistry

Hearts were fixed with paraformaldehyde (A500684, Sangon Biotech), dehydrated, embedded with paraffin, and sectioned. Hearts sections were then blocked with goat serum and incubated with primary antibodies overnight at 4℃. Then sections were incubated with secondary antibodies and Hoechst. Image analysis and quantification were performed with ImageJ as previously described [13].

Cell culture

RAW264.7 mouse macrophage cell line was purchased from Cell Lines Service. Macrophages were cultured with Dulbecco's modified Eagle's medium (10% fetal bovine serum and 1% penicillin/streptomycin). When the cell confluency reached around 80–90%, the culture medium was replaced with Dulbecco's modified Eagle's medium supplemented with EV-depleted serum. 48–72 h later, the culture medium was collected to isolate macrophages-derived EVs.

Neonatal rat ventricular cardiomyocytes (NRVCs) were isolated from the hearts of 1–3 days old Sprague Dawley rat as previously described [14]. As for hypoxia treatment, cardiomyocytes were maintained in hypoxia environment (1% O_2, 5% CO_2, and 94%N_2) for 6 h.

EV collection and isolation

The culture medium of unpolarized RAW264.7 macrophages was collected to isolate EV. The collected medium was centrifuged at 800 g for 10 min at 4 °C to remove cells and cell debris. The collected supernatant was then centrifuged at 12,000 g for 30 min at 4 °C to remove microvesicles. The supernatant was centrifuged at 150,000 g for 90 min at 4 °C, washed with PBS, and centrifuged at 150,000 g for 90 min at 4 °C again. The EV was resuspended with PBS. The amount of PBS was 1% of the volume of original culture medium. The concentration of EV solution was determined with nanoparticle tracking analysis (NTA) analysis and Pierce BCA Protein Assay Kit (Thermo Scientific, 23225).

Administration of macrophages-derived EVs

The concentration of EVs solution was about (2.36±0.34) $\times 10^8$particles/μL (determined by NTA analysis) and 446.37±28.60 ng/μL (determined by Pierce BCA Protein Assay Kit). For in vivo experiments, the macrophages-derived EVs were intramyocardially injected to mice of sham group or MI group. Mice were injected with 60–80μL EVs solution or PBS. In the MI group, after LAD ligation, the EVs solution or PBS was injected in 3–4 points around the infarcted area (the color of the infarcted myocardium was paler compared to the normal myocardium). In the sham group, the heart was exposed through the incision on the chest and then equal amount of EVs solution or PBS was injected in the same area. After operation, all mice were monitored for 3–6 h before returning to their normal animal room, and detection about cardiac function and iron metabolism were performed 24 h post operation. For in vitro experiments, EVs solution was diluted 100-fold using cell culture medium, and the same amount of PBS was added to the control group.

Electron microscopy

For transmission electron microscopy (TEM), EV solution was dropped onto the 200-mesh copper grids. Excess solution was removed after 10 min incubation. The copper grids were then incubated with 2% phosphotungstic acid hydrate for 0.5–1 min, washed with Milli-Q purified water for three times and air-dried.

For immunogold staining, EV solution was dropped onto copper grids as before. Then, EVs were fixed with paraformaldehyde for 15 min at room temperature, blocked with 5% bovine serum albumin (BSA) solution for 30 min at 37 °C, and incubated with primary antibodies for 1–2 h at 37 °C. After washing with Milli-Q purified water for three times, the grids were incubated with secondary antibodies for 1–2 h at room temperature. Then the grids were stained with 2% phosphotungstic acid hydrate as before. Antibodies used were listed below: anti-TfR (Santa Cruz, sc-65882), and Rabbit IgG control Polyclonal antibody (Proteintech, 30000-0).

All images were obtained using a transmission electron microscope (JEM-1230, JEOL Ltd., Tokyo, Japan).

Measurement of glutathione (GSH) and malondialdehyde (MDA) level

The measurement of GSH and MDA level was performed using GSH assay kit (Beyotime, S0053) and MDA assay kit (Beyotime, S0131) respectively following manufacturer's instructions.

Measurement of ROS level

The ROS measurement was performed using ROS assay kit (Beyotime, S0033) following manufacturer's instructions. Briefly, cardiomyocytes were seeded onto glass-bottomed culture dishes (NEST, 801002). After treatment, the fluorescent iron probe DCFH-DA was added to the culture medium and cells were returned to the same environment for 30 min. Then cells were washed with PBS for three times. The confocal laser-scanning microscope (Nikon A1 plus Confocal Microscope, Nikon, Japan) was used to obtain all fluorescent images, and ImageJ was used to analyze.

Measurement of cell viability

The measurement of cell viability was performed using Calcein AM cell viability assay kit (Beyotime, C2013FT) following manufacturer's instructions. The FACS Calibur flow cytometer (BD Biosciences) was used to analyze.

Dihydroxyethidium (DHE) staining

Upon harvested, the hearts were snap-frozen in liquid nitrogen. Then, the frozen hearts were embedded with OCT and sectioned. Sections were then stained with DHE and Hoechst.

Liquid chromatography tandem mass spectrometry (LC-MS/MS) analysis

EVs sample were used for MS analysis as previously described [15]. The analysis was performed using EASY-nLC 1200 UHPLC system (Thermo Fisher) and Q Exactive HF-X mass spectrometer (Thermo Fisher).

Plasmids and small interfering RNA (siRNA) construction and transfection

The TfR-EGFP and empty-EGFP plasmids were generated by Genechem. The transferrin-mcheery and empty-mCherry plasmids and siTfR were generated by Hanbio. The sequence of siTfR is CCAGACCGUUAUGUUGUA GUATT (sense) and UACUACAACAUAACGGUCUG GTT (anti-sense). Macrophages were transfected with plasmid with Lipofectamine 3000 (Invitrogen, L3000150) and were transfected with siRNA with Lipofectamine

RNAiMAX (Invitrogen, 13778500) following manufacturer's instructions.

Enzyme linked immunosorbent assay (ELISA)

The measurement of transferrin level was performed with Transferrin ELISA kit (Elabscience, E-EL-M1184c) following manufacturer's instructions.

EV tracing

EVs were labeled with Dil (Invitrogen, C7001) following manufacturer's instructions. Then, labeled EVs were intramyocardially injected. Twenty-four hours after injection, the heart, liver, spleen, skeletal muscle, lung and kidney were harvested. The harvested organs were subjected to imaging for fluorescent signal. Besides, the heart and liver were harvested, washed and frozen in liquid nitrogen. The frozen tissue was embedded with OCT and sectioned. The cell membrane was labeled with anti-ATPA1 antibody and the macrophages were labeled with anti-F4/80 antibody.

Statistical analysis

All data were expressed as mean ± standard error of mean (SEM). T-test, one-way ANOVA or 2-way ANOVA were used to analyze continuous data. All analysis was performed with GraphPad Prism 6.0 software (GraphPad Software, La Jolla, USA). $P<0.05$ indicated a statistical significance between groups.

Results

Iron overload and cell ferroptosis contributed to MI-induced cardiac injury

To stimulate acute MI injury, wild-type C57BL/6J mice were subjected to LAD coronary artery ligation. TTC staining, echocardiographic analysis and biochemical indicators detection were performed to assess the successful construction of the MI model. As shown in Fig.S1, compared to the sham group, mice undergoing MI surgery exhibited significantly increased TTC-negative area (Fig.S1a-b), decreased LVEF and LVFS, and increased LVESV and LVEDV (Fig.S1c-g). Moreover, the levels of serum markers of myocardial injury, including CK, CKMB, LDH and LDH1, were significantly increased in mice post MI (Fig.S1h-k). These findings demonstrated the successful construction of the MI model in mice.

To investigate the involvement of iron overload in cardiac injury following MI, serum iron, cardiac iron, oxidative stress indicators and ferroptosis indicators were measured. A significant increase in serum iron level was observed post MI (Fig. 1a). Additionally, cardiac iron levels also gradually increased with time post-MI surgery (Fig. 1b). The levels of transferrin and FTH1, key proteins involved in extracellular and intracellular iron storage respectively, were determined. Consistent with the trend in iron levels, both transferrin and FTH1 increased progressively over time in the MI group, peaking at 24 h post operation (Fig. 1c-d). Moreover, the hearts of MI mice exhibited increased MDA and decreased GSH levels (Fig. 1e-f), suggesting upregulated oxidative stress post MI. Notably, GPX4 and 4-hydroxynonenal (4-HNE) are hallmarks of ferroptotic cell death. As shown in Fig. 1g-j, GPX4 significantly decreased while 4-HNE significantly increased over time following MI. These results indicated that acute MI led to iron overload and ferroptosis in the myocardium, which contributed to cardiac injury and functional impairment.

Macrophage-derived EVs exhibited iron-sequestering capability

We then intended to investigate whether macrophage-derived EVs could effectively sequester iron in the myocardium. EVs were collected from the culture medium of the macrophage using ultracentrifugation. As shown in Fig. 2a, the obtained EVs were positive for EV markers, namely CD9, CD63 and TSG101, but negative for the Golgi marker GM130. TEM images revealed the typical circular morphology of EVs (Fig. 2b). Additionally, NTA revealed that the average diameter of the obtained EV was 160.43 ± 3.94 nm (Fig. 2c). To determine whether the macrophage-derived EVs possessed the capacity to sequester and remove iron, EVs were incubated with different samples including myocardium lysate, cardiomyocytes lysate, serum and cardiomyocyte culture medium (Fig. 2d). After incubation at 37℃ for 30 min, EVs were removed, and the supernatant was subjected to iron level determination. As shown in Fig. 2e-h, macrophage-derived EVs significantly reduced iron concentration in myocardium lysate, cardiomyocytes lysate, serum and cardiomyocyte culture medium, which lowered the iron levels to approximately 60–70% of the control. These results illustrated that macrophage-derived EVs possess the ability to sequester and remove iron from biological samples, making them a promising candidate for iron chelation therapy.

Macrophage-derived EVs alleviated hypoxia-induced iron overload and ferroptosis in cardiomyocytes

Having established the iron sequestration capability of macrophage-derived EVs, we investigated their efficacy in reducing MI-induced iron overload and ferroptosis. Primary NRVCs were isolated and exposed to hypoxia treatment for 6 h to mimic MI injury in vitro. Consistent with our findings in MI mice, hypoxia treatment significantly increased iron content in NRVCs and their culture medium (Fig. 3a-c). However, co-incubation with macrophage-derived EVs, but not PBS, significantly reduced the iron levels in both NRCVs and culturing medium, suggesting that macrophage-derived EVs could alleviate

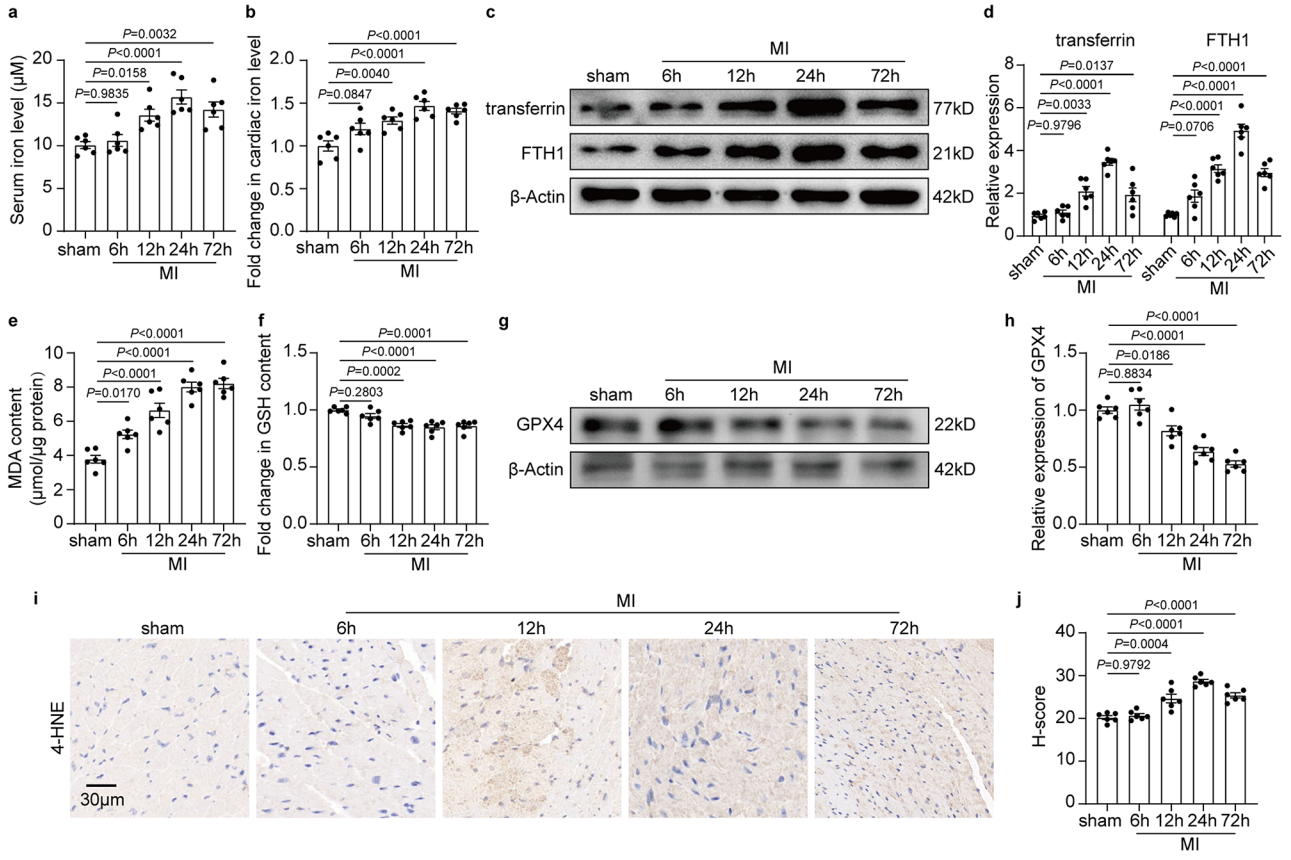

Fig. 1 Iron overload and cell ferroptosis contributes to MI-induced cardiac injury. **a** Quantitative analysis of serum iron level in sham and MI mice. **b** Quantitative analysis of cardiac iron level in sham and MI mice. **c**, **d** Representative western blotting images and quantitative analysis of transferrin and FTH1 expression in sham and MI mice. **e** Quantitative analysis of MDA level in sham and MI mice. **f** Quantitative analysis of GSH in sham and MI mice. **g**, **h** Representative western blotting images and quantitative analysis of GPX4 expression in sham and MI mice. **i**, **j** Representative immunohistochemical images and quantitative analysis of 4-HNE expression in sham and MI mice. Scale bar = 30 μm. *N* = 6 each group. Data are expressed as Mean ± SEM

hypoxia-induced iron overload in and around cardiomyocytes. Iron overload induced ferroptosis by triggering oxidative stress. As shown in Fig. 3d-f, hypoxia treatment significantly elevated the MDA and cellular ROS levels, both of which are indicators of oxidative stress. Contrastingly, the level of GSH, a crucial antioxidant enzyme, was significantly decreased (Fig. 3g). Moreover, decreased GPX4 combined with increased cell death are strong indicators of ferroptosis. As shown in Fig. 3h-l, GPX4 suppression, extensive LDH release and deceased overall cell survival were observed in hypoxia-treated NRVCs, all indicative of ferroptosis induced by iron overload in NRCVs exposed to hypoxia. Notably, macrophage-derived EVs significantly ameliorated oxidative stress and ferroptosis in hypoxia-treated NRCVs, as evidenced by decreased MDA content (Fig. 3d), reduced ROS levels (Fig. 3e-f), restored GSH level (Fig. 3g), elevated GPX4 expression (Fig. 3h-i), reduced LDH release (Fig. 3j) and improved cell survival rates (Fig. 3k-l). These results demonstrate that macrophage-derived EVs can chelate and remove excess intracellular and extracellular iron, thereby protecting cardiomyocytes against iron overload-induced oxidative stress and ferroptosis.

Macrophage-derived EVs attenuated myocardial injury by preventing iron overload in post-MI hearts

To validate the in vitro findings, macrophage-derived EVs or PBS were intramyocardially injected into mice immediately after LAD ligation, and mice were subjected to iron metabolism and cardiac function detection 24 h post operation (Fig. 4a). As shown in Fig. 4b-c, the iron levels of both serum and myocardium were increased post MI, which was consistent with our in vitro results. Meanwhile, the levels of transferrin and FTH1 were also significantly increased in the heart post MI (Fig. 4d-e). Injection of EVs reduced serum and cardiac iron levels and iron-binding protein expression in mice post-MI (Fig. 4b-e), demonstrating the ability of macrophage-derived EVs to alleviate iron overload in vivo. Moreover, indicators of oxidative stress and ferroptosis induced by MI were reversed by EV administration, as evidenced by decreased MDA content (Fig. 4f), reduced DHE

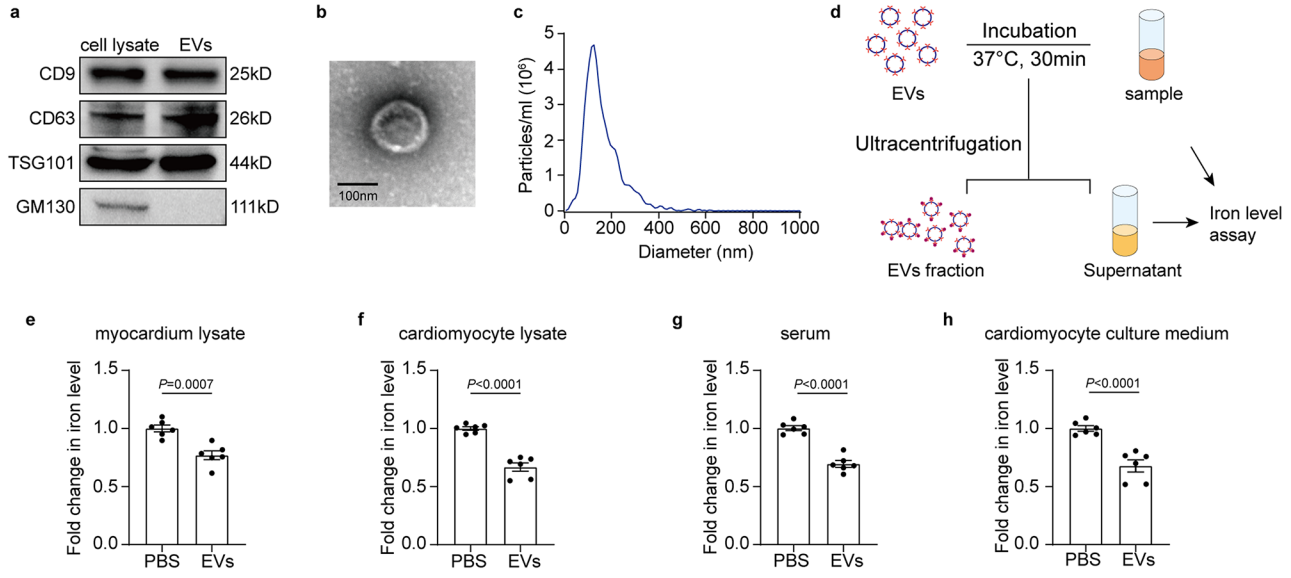

Fig. 2 Macrophage-derived EVs were capable of sequestering iron. **a** Representative western blotting image of CD9, CD63, TSG101, and GM130 expression in macrophages and macrophages-derived EVs. **b** Representative TEM images of macrophages-derived EVs. Scale bar = 100 nm. **c** NTA analysis of macrophages-derived EVs. **d** Schematic diagram of the experiment protocol to determine whether macrophages-derived EVs could sequester iron. **e-h** Quantitative analysis of iron level in myocardium lysate, cardiomyocyte lysate, serum, and cardiomyocyte culture medium after incubation with PBS or EVs. *N* = 6 each group. Data are expressed as Mean ± SEM

fluorescence density (Fig. 4g), restored GSH expression (Fig.S2a), increased GPX4 expression (Fig. 4h-i) and reduced 4-HNE levels (Fig. 4j). Finally, we evaluated the effect of macrophage-derived EVs on salvaging ischemic myocardium and improving cardiac function. TTC staining illustrated that EV treatment significantly decreased the percentage of infarcted myocardium (Fig. 4k-l). Additionally, echocardiographic results showed restored cardiac function in EV-treated post-MI mice, as indicated by increased LVEF and LVFS compared with those injected with PBS (Fig. 4m-o). The enlarged right ventricle post MI was also mitigated by EV treatment, as evidenced by decreased LVESV and LVEDV (Fig.S2 b-c). To avoid the potential interference of the cardioprotective effect of isoflurane on ischemia myocardium [16, 17], mice were also anesthetized with pentobarbital sodium. Echocardiographic results demonstrated that macrophages derived EVs showed reliable effect in improving cardiac function of MI mice regardless of the anesthetics type (Fig.S2 d-f). Furthermore, MI-induced elevation of myocardial injury biomarkers, including CK, CKMB, LDH and LDH1, was reversed by EVs injection (Fig. 4p-q, Fig. S2g-h). These data confirmed the in vivo capacity of macrophage-derived EVs in mitigating cardiac iron overload and related cardiac injury, identifying them as a highly promising candidate for endogenous biological iron chelation therapy after MI.

In addition, to investigate whether intravenous injection of EVs would achieve the therapeutic effect identical to intramyocardial injection, mice were injected with macrophage-derived EVs via the tail vein immediately after LAD ligation. Considering the non-cardiac unspecific uptake of EVs, mice with intravenous administration were injected with same amount (60–80μL each mouse) or higher amount (120–150μL each mouse) of EVs. As shown in Fig.S3, intravenous administration of EVs could not mitigate the cardiac function impairment in post-MI mice even at a higher dosage, as evidenced by comparable function indicators between MI + PBS group and intravenous injection group (Fig.S3 a-c). These data suggested that intravenous injection of EVs was not a viable option to protect against cardiac injury.

TfR was responsible for the iron-chelating capacity of macrophage-derived EVs

To elucidate the mechanism by which macrophage-derived EVs captured iron and alleviated cardiac iron overload, we examined whether EVs preferred protein-bound or labile iron. The iron in biological samples was categorized into protein-bound iron and labile iron. EVs were co-incubated with solution of iron ions (20μM). Interestingly, EV incubation failed to remove iron from the solution of iron ions (Fig. 5a), indicating that the iron-binding capacity of EVs relied on iron-binding proteins. Considering the wide distribution of receptors for iron-binding proteins on the surface of macrophages, we speculated that EVs could also inherit one or more receptors from macrophages. Hence, we performed mass spectrometry analysis on macrophage-derived EVs and results revealed the presence of TfR, a critical receptor

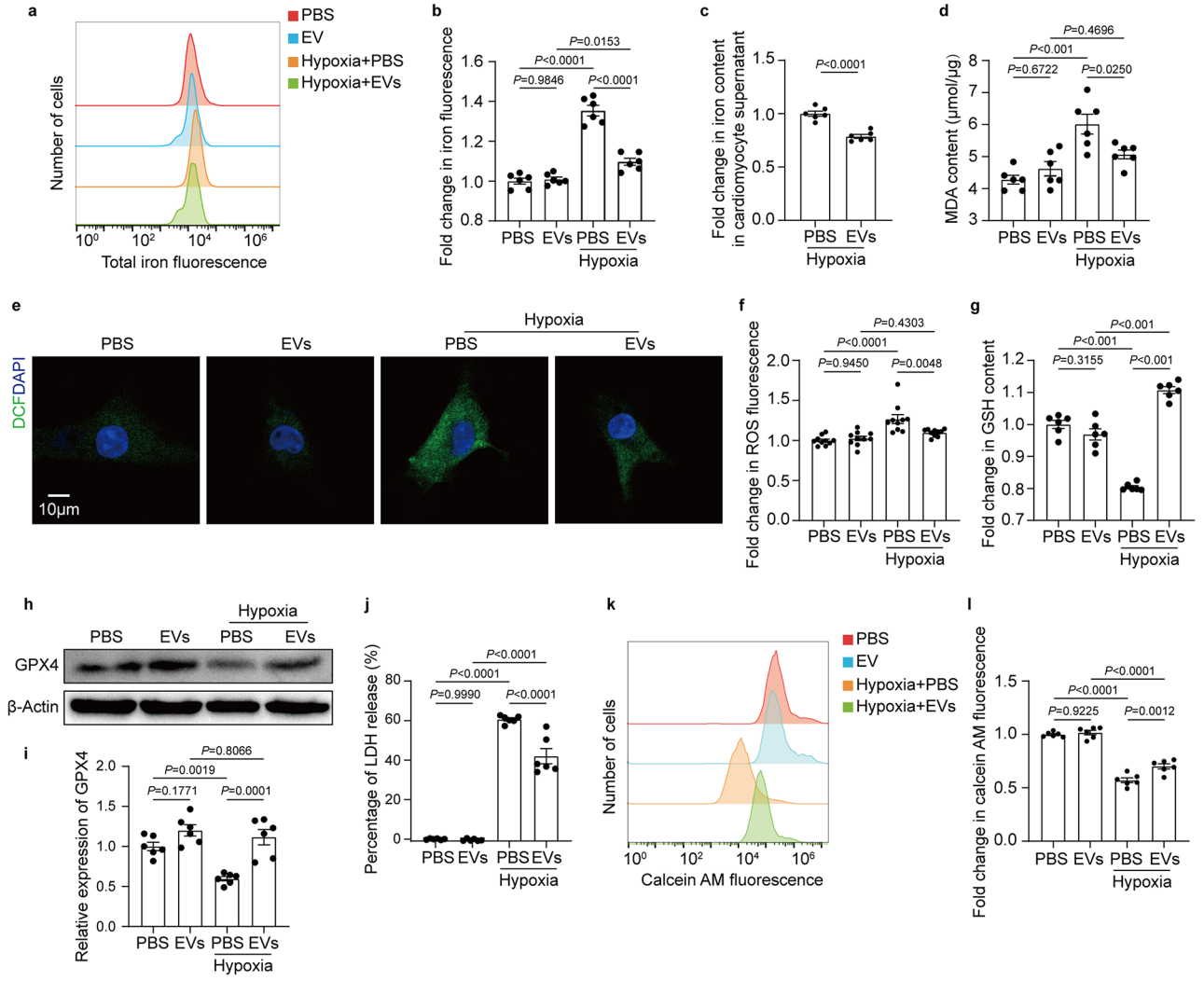

Fig. 3 Macrophage-derived EVs alleviated hypoxia-induced iron overload and ferroptosis in cardiomyocytes. **a-b** Representative flow cytometer results and quantitative analysis of cellular iron. **c** Quantitative analysis of iron level in culture medium of hypoxia cardiomyocytes treated with PBS or EVs. **d** Quantitative analysis of MDA level in cardiomyocytes. **e**, **f** Representative images and quantitative analysis of cellular ROS level. Scale bar = 10 μm. **g** Quantitative analysis of GSH level in cardiomyocytes. **h**, **i** Representative western blotting images and quantitative analysis of GPX4 expression in cardiomyocytes. **j** Quantitative analysis of released LDH level in cardiomyocytes. **k**, **l** Representative flow cytometer results and quantitative analysis of cardiomyocytes positive for calcein AM. *N* = 6 each group. Data are expressed as Mean ± SEM

for transferrin-mediated cellular iron uptake, on macrophage-derived EVs. Western blotting and immunogold staining confirmed the presence and enrichment of TfR on macrophage-derived EVs (Fig. 5b-c).

Next, we investigated the origin of TfR on the surface of EVs by transfecting macrophages with a plasmid expressing EGFP-labelled TfR. Fluorescence intensity was significantly increased in the culture medium of TfR-EGFP plasmid-transfected macrophages compared to those transfected with an empty EGFP plasmid. (Fig. 5e). Moreover, EVs released by TfR-EGFG plasmid-transfected macrophages exhibited significant enrichment of EGFP fluorescence (Fig. 5f-g), suggesting that EGFP-labelled TfR was secreted by macrophages in the form of EVs. Furthermore, we constructed a plasmid expressing mCherry labelled transferrin to confirm whether macrophage-derived EVs could bind transferrin. The experimental design is illustrated in Fig. 5h. Briefly, lysate of cells transfected with transferrin-mCherry plasmid or empty-mCherry plasmid were collected and EVs with TfR-EGFP were incubated with either lysate. As shown in Fig. 5i, the mCherry fluorescence intensity of EVs incubated with transferrin-mCherry lysate was significantly increased compared to EVs incubated with empty-mCherry lysate, demonstrating the TfR on the surface of EVs could bind to transferrin. To further determine the biological function of the TfR-transferrin binding, we determined the transferrin level in myocardium lysate, serum, cardiomyocyte lysate and cardiomyocyte culture medium post incubation with EVs or PBS. Compared to

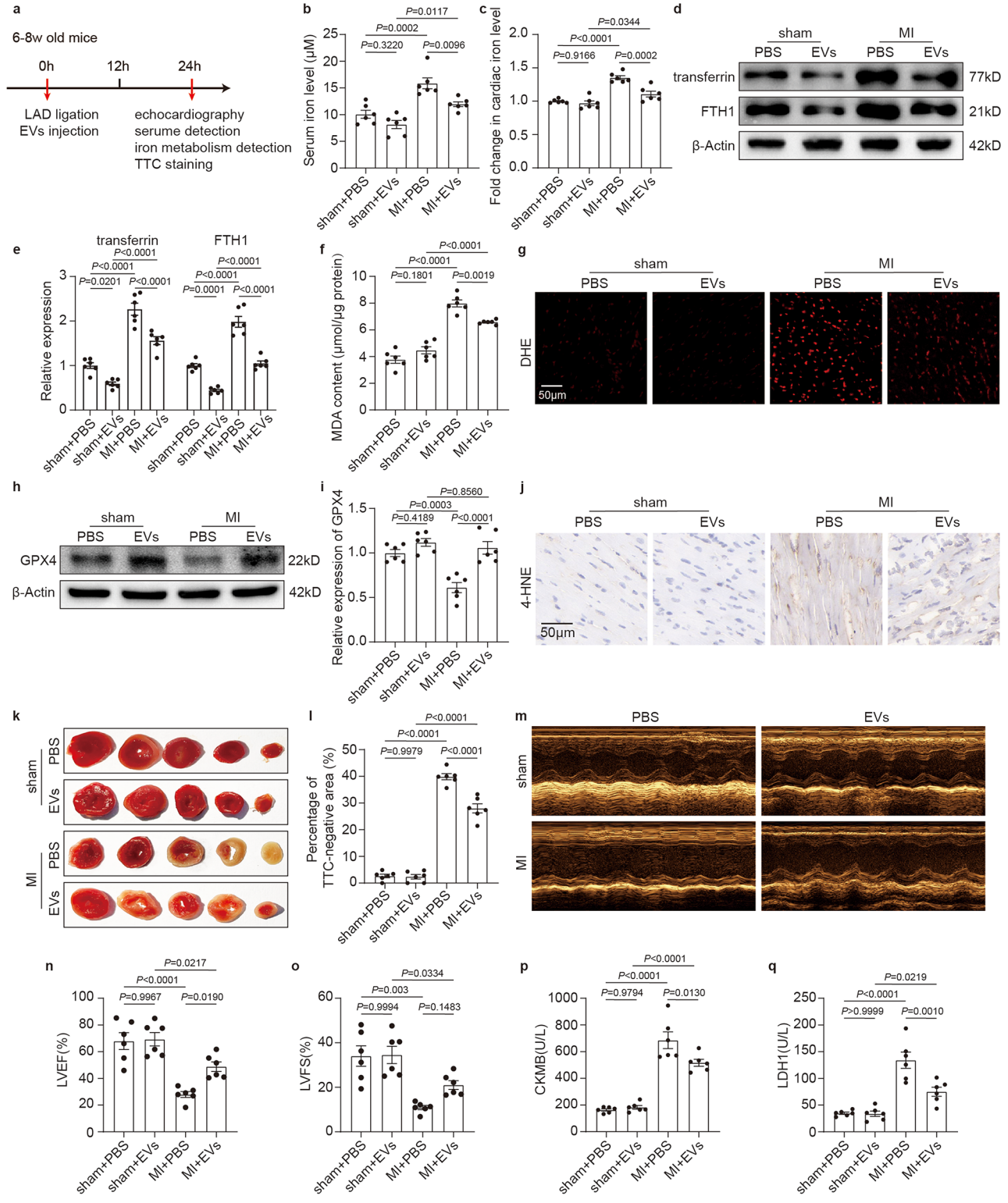

Fig. 4 Macrophage-derived EVs attenuated myocardial injury by preventing iron overload in post-MI heart. **a** Diagram of MI construction and EVs injection protocol. **b** Quantitative analysis of serum iron level in mice. **c** Quantitative analysis of cardiac iron level in mice. **d**, **e** Representative western blotting images and quantitative analysis of transferrin and FTH1 expression in hearts of mice. **f** Quantitative analysis of MDA level in hearts of mice. **g** Representative DHE staining images of hearts of mice. Scale bar = 50 μm. **h**, **i** Representative western blotting images and quantitative analysis of GPX4 expression in hearts of mice. **j** Representative immunohistochemical images of 4-HNE expression in hearts of mice. Scale bar = 50 μm. **k**, **l** Representative TTC staining images and quantitative analysis of infarcted area of hearts. **m** Representative M-mode echocardiography images. **n**, **o** Quantitative analysis of LVEF and LVFS. **p**, **q** Quantitative analysis of serum CKMB and LDH1 in mice. *N* = 6 each group. Data are expressed as Mean ± SEM

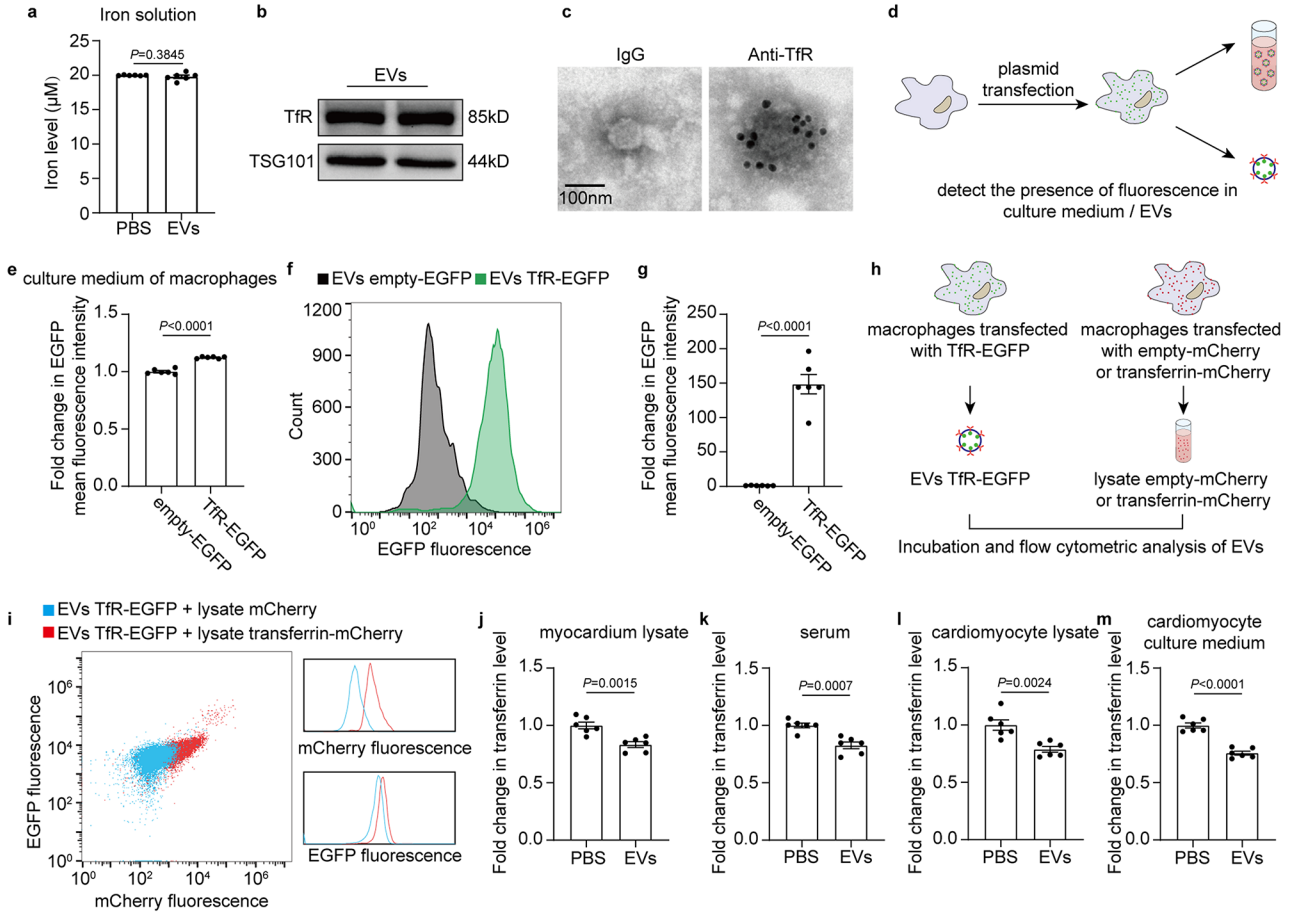

Fig. 5 TfR was responsible for the iron-chelating capacity of macrophages-derived EVs. **a** Quantitative analysis of iron level in iron solution after incubation with PBS or EVs. **b** Representative western blotting images of TfR expression in macrophages-derived EVs. **c** Representative immunogold TEM images of macrophages-derived EVs incubated with IgG or anti-TfR. Scale bar = 100 nm. **d** Schematic diagram of the experiment protocol to determine the origin of TfR on EVs. **e** Quantitative analysis of fluorescence intensity of culture medium. **f**, **g** Representative flow cytometer results and quantitative analysis of fluorescence intensity of EVs released by macrophages transfected with empty-EGFP or TfR-EGFP plasmid. **h** Schematic diagram of the experiment protocol to determine whether TfR on EVs could bind with transferrin. **i** Representative flow cytometer results of EVs released by macrophages transfected with TfR-EGFP plasmid after incubation with cell transfected with transferrin-mCherry or empty-mCherry plasmid. **j-m** Quantitative analysis of transferrin level of myocardium lysate, serum, cardiomyocytes lysate, and culture medium of cardiomyocytes after incubation with macrophages-derived EVs. *N* = 6 each group. Data are expressed as Mean ± SEM

PBS incubation, EV incubation significantly reduced the transferrin level in all these samples (Fig. 5j-m), illustrating that the macrophage-derived EVs could capture and remove excess transferrin by binding with it. Collectively, these results demonstrated that the interaction between EV-resident TfR and transferrin provides a molecular basis for the iron chelating capacity of macrophage-derived EVs, thereby alleviating iron overload.

EVs released by TfR-deficient macrophages lost their iron-chelating capacity and cardiac protective effect against MI

To further confirm the essential role of TfR in the cardioprotective effect of macrophage-derived EVs, we constructed small interfering RNA targeting TfR (siTfR) and transfected it into macrophages. As shown in Fig. 6a, transfection of siTfR significantly reduced TfR expression in macrophages. Moreover, the knockdown of TfR in macrophages resulted in a deficiency of TfR in macrophage-derived EVs (Fig. 6a). Then, EVs released by macrophages transfected with negative control (EVs-siNC) or si-TfR (EVs-siTfR) were collected and intramyocardially injected into post-MI hearts. Similar to our in vivo results of normal macrophage-derived EVs, the injection of EVs-siNC alleviated MI-induced iron overload in the serum and myocardium (Fig. 6b-c). However, this iron-chelating effect was lost in mice injected with EVs-siTfR, as evidenced by comparable iron levels in serum and myocardium between mice injected with PBS and EVs-siTfR (Fig. 6b-c). Further detection of iron-binding protein also revealed that EV-siTfR failed in suppressing the upregulation of iron-binding proteins induced by MI (Fig. 6d-e), suggesting that TfR was essential for

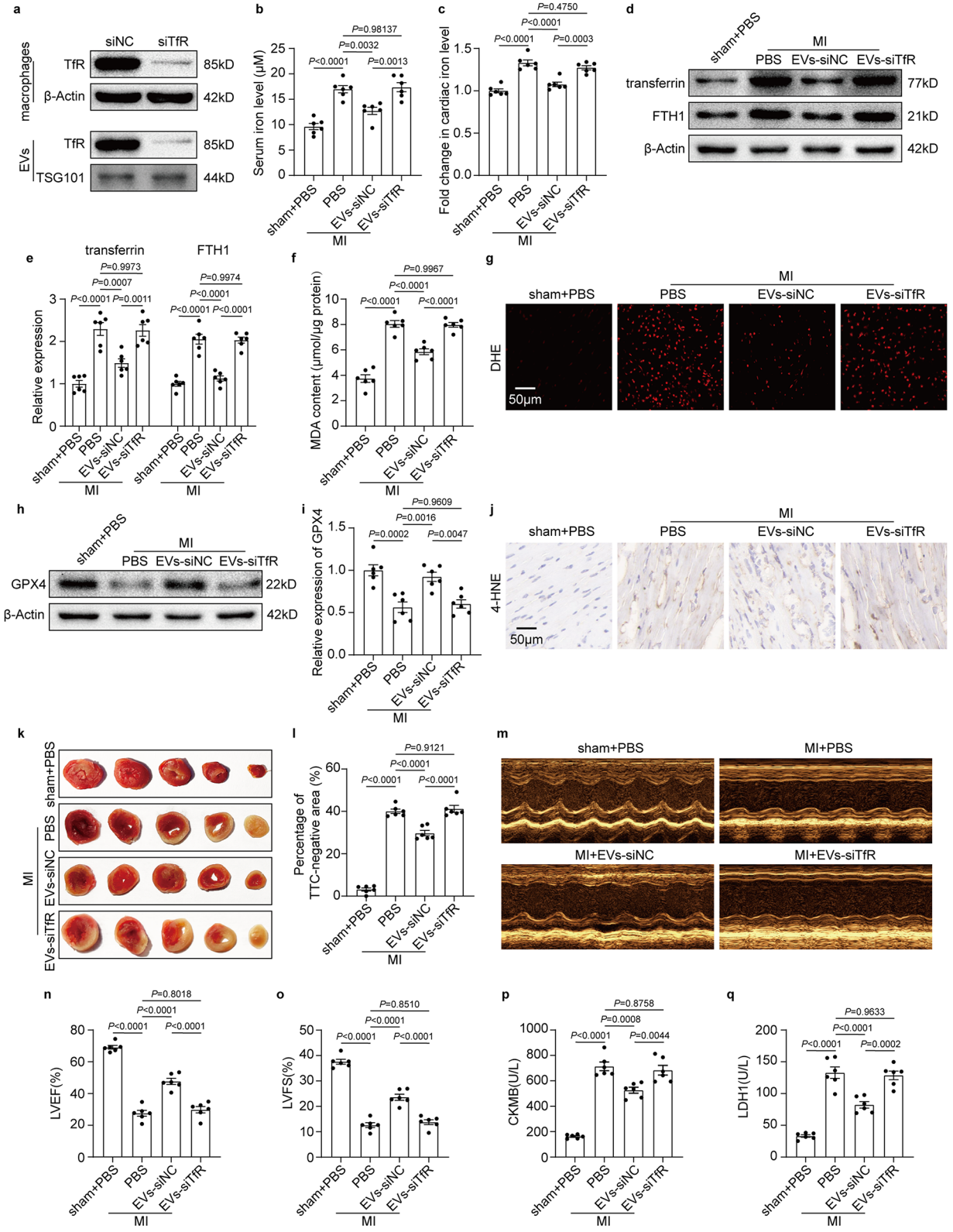

Fig. 6 (See legend on next page.)

(See figure on previous page.)

Fig. 6 EVs released by macrophages with TfR deficiency exhibited reduced cardiac protective effect against MI. **a** Representative western blotting images of TfR expression in macrophages transfected with siTfR and EVs released by such macrophages. **b** Quantitative analysis of serum iron level of mice. **c** Quantitative analysis of cardiac iron level of mice. **d**, **e** Representative western blotting images and quantitative analysis of transferrin and FTH1 expression in hearts of mice. **f** Quantitative analysis of MDA level of mice. **g** Representative DHE staining images of hearts of mice. Scale bar = 50 μm. **h**, **i** Representative western blotting images and quantitative analysis of GPX4 expression in hearts of mice. **j** Representative immunohistochemical images of 4-HNE expression in hearts of mice. Scale bar = 50 μm. **k**, **l** Representative TTC staining images and quantitative analysis of infarcted area of hearts. **m** Representative M-mode echocardiography images. **n**, **o** Quantitative analysis of LVEF and LVFS. **p**, **q** Quantitative analysis of serum CKMB and LDH1 in mice. *N* = 6 each group. Data are expressed as Mean ± SEM

the ability of macrophage-derived EVs in chelating iron and preventing iron overload. Moreover, EVs-siTfR also failed to protect against MI-induced oxidative stress and cardiomyocytes ferroptosis, as indicated by no significant difference in indicators such as MDA levels (Fig. 6f), DHE fluorescence density (Fig. 6g), GPX4 expression (Fig. 6h-i) and 4-HNE levels (Fig. 6j) between mice injected with PBS and EVs-siTfR. Cardiac infarcted size and cardiac function were further determined. TTC staining revealed that injection of EVs-siNC significantly reduced the percentage of TTC-negative area in post-MI mice, which was abolished in MI mice injected with EVs-siTfR (Fig. 6k-l). Additionally, echocardiographic results demonstrated that EVs-siTfR treatment could not mitigate the cardiac function impairment in post-MI mice, as evidenced by comparable function indicators including LVEF, LVFS, LVESV and LVEDV between mice injected with PBS and EVs-siTfR (Fig. 6m-o and Fig.S4a-b). Besides, the excessively elevated myocardial injury markers, including CK, CKMB, LDH and LDH1, showed no significant reduction after the administration of EVs-siTfR (Fig. 6p-q and Fig. S4c-d). Collectively, these results demonstrated that EVs released by TfR-deficient macrophages could not alleviate cardiac iron overload, relieve ferroptosis and restore cardiac function, highlighting the indispensable role of TfR on macrophage-derived EVs in their protective effect against MI-induced myocardial injury.

Iron-chelating EVs were captured and further processed by macrophages in the liver

To further identify the temporal and spatial distribution of macrophages derived EVs post intramyocardial injection and iron chelation, we labelled EVs with fluorescent dye Dil and then performed in vivo imaging and immunofluorescence detection. As shown in Fig. 7a, the Dil signal maintained at a high level in heart for 3 h post injection, and gradually reduced and nearly disappeared until 6 h post injection. Further immunofluorescence results demonstrated that the majority of Dil labelled EVs were present in extracellular space of the heart (Fig. S5a, indicated by solid arrow), while a small fraction of EVs were captured by cardiomyocytes (labelled by cTnT), fibroblasts (labelled by αSMA), and endothelial cells (labelled by CD31) (Fig.S5a, indicated by dotted arrow). Then we investigated which organ was responsible for processing the iron-chelating EVs released from the heart. In vivo imaging results showed that the Dil-fluorescent signal was significantly enriched in the liver (Fig. S5b), while other organs, including spleen, skeletal muscle, lung and kidney, showed a minimal fluorescent signal 24 h post the EVs injection (Fig.S5b). Further immunofluorescence detection also revealed that Dil signals were present in the liver of mice intramyocardially injected with Dil-labelled EVs (Fig.S5c). Next, we detected time-dependent change of Dil-fluorescent signal in the liver. As shown in Fig. 7b, the Dil fluorescence signal in the liver tissue reached its peak 6 h after intramyocardial EVs injection. The increase of fluorescent signal in liver was coordinated with the decrease of that in heart, indicating that the iron-chelating EVs released from myocardium were further processed by the liver. Moreover, when compared to MI mice injected with PBS, administration of macrophages derived EVs increased the iron content in the liver (Fig. 7c), further suggesting the liver as the main target organ for EV processing. Finally, we elucidate the specific liver-resident cell in charge of processing iron-chelating EVs. As shown in Fig. 7d, fluorescence staining showed that EVs (labelled by Dil, red) exhibited co-localization with macrophages (labelled by F4/801, green). These results demonstrated that liver-resident macrophages were the primary cell type involved in capturing and processing iron-chelating EVs in post-MI mice.

Discussion

In this study, we identified macrophage-derived EVs as a novel endogenous biological chelator for excess iron (Fig. 8). The application of macrophage-derived EVs in hypoxic cardiomyocytes and post-MI hearts showed significant effects in preventing oxidative stress and ferroptosis induced by iron overload. Moreover, we also identified TfR on EVs as the key player responsible for binding with transferrin and removing protein-bound iron. EVs with TfR deficiency lost their iron-chelating capacity and cardioprotective effect in post-MI hearts. Additionally, we discovered that iron-chelating EVs were ultimately captured and processed by macrophages in the liver. Our work provides in vitro and in vivo evidence for macrophage-derived EVs as a powerful endogenous tool for iron chelation therapy, which reveals a novel and promising therapeutic approach for protecting against iron overload-induced injury in the pathogenesis of MI and other cardiovascular diseases.

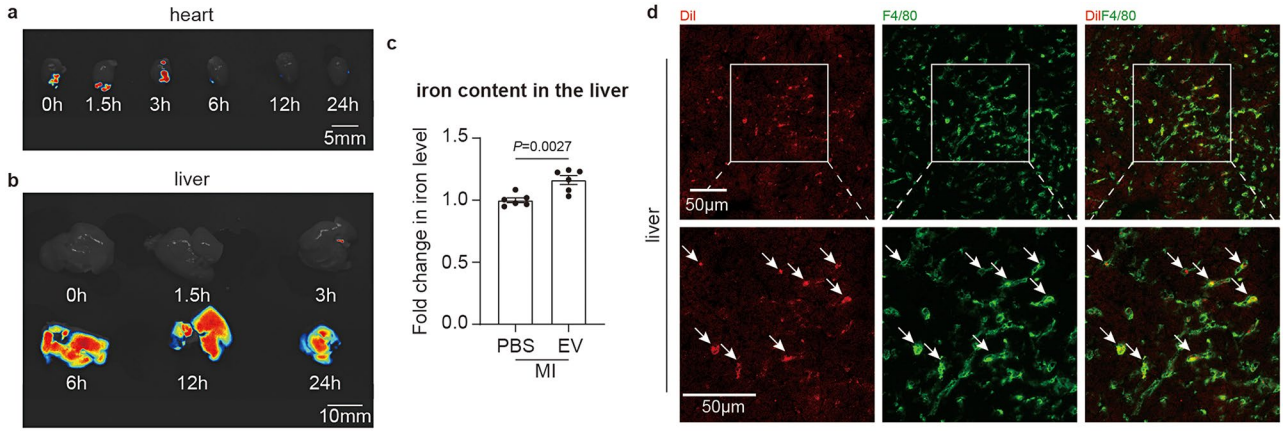

Fig. 7 Macrophages-derived EVs were captured by macrophages in liver. **a** Representative live imaging results of distribution of Dil-labeled EVs in the heart. **b** Representative live imaging results of distribution of Dil-labeled EVs in the liver. **c** Quantitative analysis of liver iron level of mice. **d** Representative fluorescent images of the liver. EVs were labeled with Dil and macrophages were labeled with F4/80. Scale bar = 50 μm

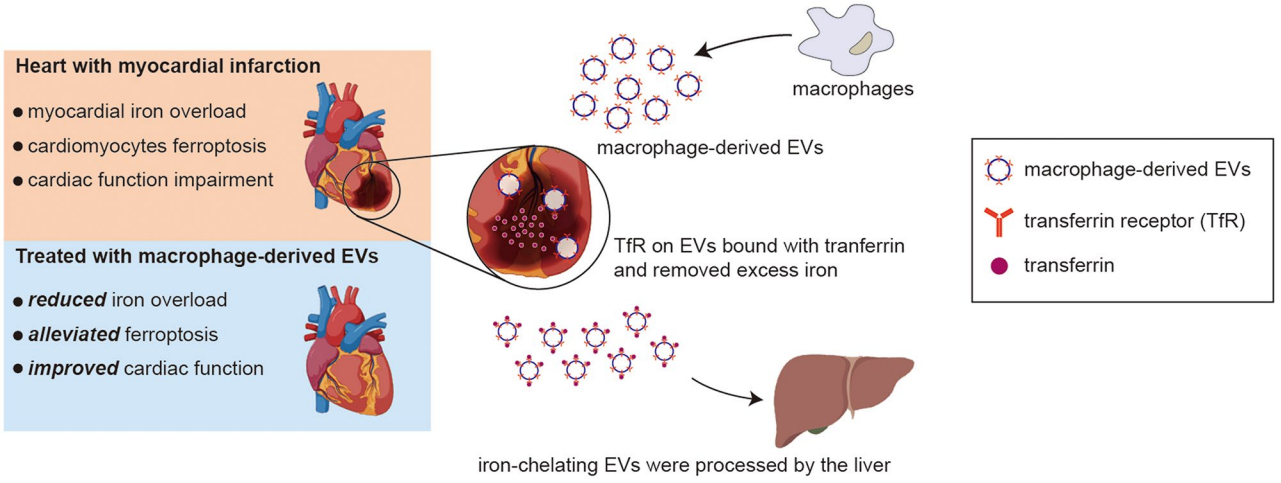

Fig. 8 Schematic figure illustrating the mechanism underlying the therapeutic effect of macrophage-derived EVs on MI. Myocardial iron overload, cardiomyocytes ferroptosis, and cardiac function impairment were detected in the hearts post MI, which contributed to the poor prognosis of MI. This work identified that macrophage-derived EVs exhibited protective effect on reducing myocardial iron overload, alleviating cardiomyocytes ferroptosis, and improving cardiac function post MI. Mechanistically, TfR on macrophage-derived EVs was the key player responsible for binding with transferrin and removing protein-bound iron. These iron-chelating EVs were ultimately captured and processed by macrophages in the liver

Many studies have reported the existence of iron overload in ischemic myocardium. Using cardiac magnetic resonance imaging, researchers observed the iron deposition in the myocardium of patients with ST-elevation myocardial infarction (STEMI), both at the early stage (within a week) and the late stage (approximately 5–6 months) post STEMI [2, 6]. Animal experiments further demonstrated that both labile and protein-bound iron exhibited a significant increase in infarcted hearts, accompanied by a significant upregulation of proteins responsible for iron binding, including ferritin light chain (FLC), FTH1 and haemoglobin [18]. In this study, we also observed an increase in the total iron and the upregulation of FTH1 in MI hearts. Besides, we also confirmed that transferrin, another iron-binding protein, was increased post MI. These findings suggested that multiple forms of iron are deposited in the heart during the development of MI, with protein-bound iron accounting for a significant portion. Under normal conditions, transferrin binding of iron maintains an extremely low concentration of free iron, thus avoiding free-iron-induced oxidative damage. However, during cardiac ischemia, iron released by ruptured and damaged cardiomyocytes are further oxidized by ceruloplasmin and bound to transferrin [19, 20], leading to the deposition of both free iron and protein-bound iron. Our study further demonstrated that the removal of transferrin-bound iron by EVs could significantly prevent MI-induced iron overload and protect against cardiac injury, indicating the detrimental role of excess transferrin-bound iron in the pathogenesis of MI. Although free iron (non-transferrin-bound iron) has been considered to be harmful, our study revealed

that the deposition of transferrin-bound iron in a locally injured organ has deleterious effects.

Macrophages not only regulate iron metabolism but also play a crucial role in regulating post-MI inflammation. Studies report that pro-inflammatory macrophages dominate the early stage after MI, triggering inflammatory damage, while the proliferation of anti-inflammatory macrophages drives post-MI repair and long-term ventricular remodelling at the late stage [21]. Moreover, it is well-established that the early activation of macrophages after MI would exacerbate tissue damage and lead to the expansion of the infraction area [22], highlighting that macrophages play a negative role in the early-stage post MI. However, our study discovered that the administration of EVs released by macrophages, which were not polarised, exerted remarkable iron sequestering capacity and cardioprotective effect in the early phase post MI. Furthermore, a previous study reported that EVs released by macrophages post-bacterial infection, which might exhibit a proinflammatory phenotype, also possessed iron sequestering capacity [10]. These results suggest that the cardioprotective iron sequestering mechanism might exist in the macrophages during the early-stage post MI but can be overridden by the proinflammatory adverse role. Moreover, we discovered that liver-resident macrophages were also involved in iron handling after MI injury, wherein intramyocardial iron-chelated EVs were further captured and processed by liver-resident macrophages. Hepatocellular iron uptake is an important determinant of the overall iron homeostasis of the organism. Considering the primary role of the liver in systematic iron regulation, we speculated that liver-recycled iron was further processed and re-entered the iron cycling. Collectively, our study revealed a macrophage-based endogenous mechanism governing the cross-organ iron transport, which is important to maintain iron homeostasis when encountering acute local iron overload.

Furthermore, we discovered that the iron-chelating capacity of macrophage-derived EVs relies on the TfR on their surface. Through the interaction of ligands and receptors, EV-resident TfR was able to capture and remove the transferrin-bound iron in serum and ischemia myocardium. Conversely, TfR-deficient EVs lost their capacity to decrease cardiac iron levels and mitigate ischemia myocardial injury. Previous studies have demonstrated that EVs play a role in cell-cell or cell-extracellular space communication by delivering vesicle content, including proteins, nucleic acid or even organelles. Our study provides visible evidence that the protein on the surface of macrophage-derived EVs, specifically the receptor protein TfR, plays a crucial role in their function rather than the vesicle content. In the last decade, EVs, especially exosomes, were artificially modified to deliver their content to target organs or cells, wherein EVs acquired additional functions. The artificially modified EVs serve as a potential intervention strategy for targeted therapy of many diseases. Alternatively, our findings regarding macrophage-derived EVs inspired a novel optional strategy for EV modification. By assembling different receptors or ligands on their surface, EVs can act as a carrier and acquire the bioactivity of target proteins. Taken together, our study revealed a novel mechanism by which EVs perform their function, suggesting that the surface of EVs has the potential for modification. Considering the important role of macrophages in iron metabolism regulation, macrophage was chosen as the source of EVs in the present study. Other cell types including adipose-derived mesenchymal stem cells (ADSCs) and HEK293T cells, which was recently frequently used for EVs collection, might be also suitable candidate for EVs collection after appropriate modification.

Despite the important insights, this study has certain limitations. For instance, the relationship between the levels of TfR in macrophages and EVs is still unclear. As we have demonstrated that TfR deletion in macrophages could significantly decrease the level of EV-resident TfR, it would be more compelling to see an elevated EV-resident TfR level after TfR overexpression on their parent cells. Moreover, in this study, the macrophage-derived EVs were intramyocardially injected, which limits its clinical applicability. Notably, tail vein injection of biological agents targeting the heart was reported to have good efficacy in protecting against multiple cardiac diseases. Therefore, strategies are required to improve the cardiac direction of macrophage-derived EVs.

Conclusion

In conclusion, we discovered that macrophages-derived EVs were an effective and novel endogenous iron chelating therapy. Administration of macrophages-derived EVs significantly alleviated MI-induced iron overload, ferroptosis, and cardiac function impairment. Moreover, we illustrated that the TfR, which was inherited from macrophages to the surface of EVs, interacted with transferrin and removed excess transferrin-bound iron, fostering the cardioprotective effect of macrophages-derived EVs. In summary, our work identified a novel mechanism of EVs function, which provides a promising therapeutic candidate for treating iron overload-induced injury in MI and other diseases.

Abbreviations

4-HNE	4-hydroxynonenal
CK	Creatine kinase
DFO	Deferoxamine
DFP	Deferiprone
DFX	Deferasirox
EVs	Extracellular vesicles
EVs-siNC	Extracellular vesicles released by macrophages transfected with negative control

EVs-siTfR	Extracellular vesicles released by macrophages transfected with si-TfR
FLC	Ferritin light chain
FTH1	Ferritin heavy chain 1
GPX4	Glutathione peroxidase 4
GSH	Glutathione
LAD	Left anterior descending
LDH	Lactate dehydrogenases
LVEDV	Left ventricular end-diastolic volume
LVEF	Left ventricular ejection fraction
LVESV	Left ventricular end-systolic volume
LVFS	Left ventricular fractional shortening
MDA	Malondialdehyde
MI	Myocardial infarction
NTA	Nanoparticle tracking analysis
NRVCs	Neonatal rat ventricular cardiomyocytes
ROS	Reactive oxygen species
STEMI	ST-elevation myocardial infarction
TEM	Transmission electron microscopy
TfR	Transferrin receptor
TTC	Triphenyl tetrazolium chloride

Supplementary Information

The online version contains supplementary material available at https://doi.org/10.1186/s12951-024-02800-1.

Supplementary Material 1

Acknowledgements
We thank Bullet Edits Limited for the linguistic editing of the manuscript.

Author contributions
DG, XY, and RY contributed equally to this work. DG, XY, RY, and LH conceived and designed the experiments; DG, XY, RY, JG, XZ, YW, TP, ML, QL, SP and ZL performed all the experiments; XY, RY, JG, XZ and YW analyzed and discussed the data; DG and XY wrote the manuscript; FF, LH and YL revised and finalized the manuscript.

Funding
This work was supported by the grants from the National Natural Science Foundation of China (grant no.82070385 and grant no. 82200404).

Data availability
The data that support the findings of this study are available from the corresponding author upon reasonable request.

Declarations

Ethics approval and consent to participate
Protocols of animal experiments included in this study were approved by the policies and guidelines of the Animal Ethics Committee of Air Force Medical University.

Consent for publication
All authors confirmed that this work has not been published before, and was not under consideration for publication elsewhere. All authors have approved the submission of this manuscript to *Journal of Nanobiotechnology*.

Competing interests
The authors declare no competing interests.

Received: 19 March 2024 / Accepted: 22 August 2024
Published online: 31 August 2024

References

1. Tsao CW, Aday AW, Almarzooq ZI, Alonso A, Beaton AZ, Bittencourt MS, et al. Heart Disease and Stroke Statistics-2022 update: a Report from the American Heart Association. Circulation. 2022;145:e153–639.
2. Bulluck H, Rosmini S, Abdel-Gadir A, White SK, Bhuva AN, Treibel TA, et al. Residual myocardial Iron following intramyocardial hemorrhage during the Convalescent Phase of Reperfused ST-Segment-Elevation myocardial infarction and adverse left ventricular remodeling. Circ Cardiovasc Imaging. 2016;9:e004940.
3. Miyamoto HD, Ikeda M, Ide T, Tadokoro T, Furusawa S, Abe K, et al. Iron Overload via Heme Degradation in the endoplasmic reticulum triggers ferroptosis in myocardial ischemia-reperfusion Injury. JACC Basic Transl Sci. 2022;7:800–19.
4. Pantopoulos K, Porwal SK, Tartakoff A, Devireddy L. Mechanisms of mammalian iron homeostasis. Biochemistry. 2012;51:5705–24.
5. Fang X, Ardehali H, Min J, Wang F. The molecular and metabolic landscape of iron and ferroptosis in cardiovascular disease. Nat Rev Cardiol. 2023; 20.
6. Carberry J, Carrick D, Haig C, Ahmed N, Mordi I, McEntegart M, et al. Persistent Iron within the Infarct Core after ST-Segment Elevation myocardial infarction: implications for left ventricular remodeling and Health outcomes. JACC Cardiovasc Imaging. 2018;11:1248–56.
7. Feng W, Xiao Y, Zhao C, Zhang Z, Liu W, Ma J, et al. New Deferric Amine compounds efficiently chelate excess Iron to treat Iron Overload disorders and to prevent ferroptosis. Adv Sci (Weinh). 2022;9:e2202679.
8. Ribeiro LB, Soares EA, Costa FF, Gilli SCO, Olalla Saad ST, Benites BD. The challenges of handling deferasirox in sickle cell disease patients older than 40 years. Hematology. 2019;24:596–600.
9. Corna G, Caserta I, Monno A, Apostoli P, Manfredi AA, Camaschella C, et al. The repair of skeletal muscle requires Iron Recycling through Macrophage Ferroportin. J Immunol. 2016;197:1914–25.
10. Kuang H, Dou G, Cheng L, Wang X, Xu H, Liu X, et al. Humoral regulation of iron metabolism by extracellular vesicles drives antibacterial response. Nat Metab. 2023;5:111–28.
11. Gao E, Lei YH, Shang X, Huang ZM, Zuo L, Boucher M, et al. A novel and efficient model of coronary artery ligation and myocardial infarction in the mouse. Circ Res. 2010;107:1445–53.
12. Hu L, Guo Y, Song L, Wen H, Sun N, Wang Y, et al. Nicotinamide riboside promotes Mfn2-mediated mitochondrial fusion in diabetic hearts through the SIRT1-PGC1α-PPARα pathway. Free Radic Biol Med. 2022;183:75–88.
13. Paschalis A, Sheehan B, Riisnaes R, Rodrigues DN, Gurel B, Bertan C, et al. Prostate-specific membrane Antigen Heterogeneity and DNA repair defects in prostate Cancer. Eur Urol. 2019;76:469–78.
14. Hu L, Ding M, Tang D, Gao E, Li C, Wang K, et al. Targeting mitochondrial dynamics by regulating Mfn2 for therapeutic intervention in diabetic cardiomyopathy. Theranostics. 2019;9:3687–706.
15. Qi B, He L, Zhao Y, Zhang L, He Y, Li J, et al. Akap1 deficiency exacerbates diabetic cardiomyopathy in mice by NDUFS1-mediated mitochondrial dysfunction and apoptosis. Diabetologia. 2020;63:1072–87.
16. Zhou R, Jia Y, Wang Y, Li Z, Qi J, Yang Y. Elevating miR-378 strengthens the isoflurane-mediated effects on myocardial ischemia-reperfusion injury in mice via suppression of MAPK1. Am J Transl Res. 2021;13:2350–64.
17. Huang H, Qing X, Li H. Isoflurane Preconditioning protects the Myocardium against Ischemia and Reperfusion Injury by Upregulating GRM1 expression. Curr Neurovasc Res. 2020;17:171–6.
18. Moon BF, Iyer SK, Hwuang E, Solomon MP, Hall AT, Kumar R, et al. Iron imaging in myocardial infarction reperfusion injury. Nat Commun. 2020;11:3273.
19. Winn NC, Volk KM, Hasty AH. Regulation of tissue iron homeostasis: the macrophage ferrostat. JCI Insight. 2020; 5.
20. Musci G, Polticelli F, Bonaccorsi di Patti MC. Ceruloplasmin-ferroportin system of iron traffic in vertebrates. World J Biol Chem. 2014;5:204–15.
21. Yap J, Irei J, Lozano-Gerona J, Vanapruks S, Bishop T, Boisvert WA. Macrophages in cardiac remodelling after myocardial infarction. Nat Rev Cardiol. 2023;20:373–85.
22. Frantz S, Bauersachs J, Ertl G. Post-infarct remodelling: contribution of wound healing and inflammation. Cardiovasc Res. 2009;81:474–81.

Publisher's note